Chapter 11
Shaker Testing of a Fuel Cell Stack: Modal Survey, FE Model Updating, and Fixture Coupling Neutralization

Giancarlo Kosova, Vittoria D'Alessio, Emilio Di Lorenzo, Lorenzo Dozio, Simone Gallas, Hervé Denayer, Giovanni Fasulo, Mattia Barbarino, and Oskar Ekblad

Abstract This paper presents a comprehensive study of a fuel cell stack's dynamic behavior through shaker testing, focusing on experimental characterization and numerical model validation. The investigation was conducted as part of a design campaign to ensure structural integrity under operational conditions.

The study pursued four main objectives: (1) conducting preliminary environmental tests on single and multi-axis shaker platforms to assess structural durability, (2) performing experimental modal analysis to extract mode shapes and frequencies, (3) updating and validating a finite element model (FEM) for structural integrity predictions, and (4) developing decoupling procedures to neutralize the dynamic interaction between the test structure and the fixture/slip table assembly.

The investigation yielded several key results. The preliminary environmental tests successfully validated control-loop stability across different stack configurations. The modal survey, using table acceleration as a reference, revealed amplitude-dependent behavior indicative of structural nonlinearities. Despite having detailed design information, the initial finite element model showed significant discrepancies compared to experimental data. Through model updating based on the experimental modal model, these differences were substantially reduced, achieving excellent correlation in natural frequencies and mode shapes, while transmissibility functions showed good but not perfect agreement. Various substructuring methods were implemented to extract the fixed-base characteristics of the fuel cell stack, and while they partially corrected both natural frequencies and mode shapes, their effectiveness demonstrated considerable sensitivity to the specific approach and parameters employed.

The results illustrate the fundamental importance of shaker testing in the design process of fuel cell stacks, providing crucial insights into their dynamic behavior and enabling the development of reliable numerical models for durability predictions.

Keywords Shaker testing · EMA · FEM · Decoupling

Giancarlo Kosova · Vittoria D'Alessio · Emilio Di Lorenzo
Siemens Digital Industries Software, Leuven, Belgium
e-mail: giancarlokosova@siemens.com; dalessiovittoria1@gmail.com; emilio.dilorenzo@siemens.com

Vittoria D'Alessio · Lorenzo Dozio
Politecnico di Milano, Milan, Italy
e-mail: dalessiovittoria1@gmail.com; lorenzo.dozio@mail.polimi.it

Simone Gallas · Hervé Denayer
KU Leuven, Department of Mechanical Engineering, Heverlee, Belgium
e-mail: simone.gallas@kuleuven.be; herve.denayer@kuleuven.be

Simone Gallas · Hervé Denayer
Flanders Make, Flanders Make@KU Leuven, Belgium
e-mail: simone.gallas@kuleuven.be; herve.denayer@kuleuven.be

Giovanni Fasulo · Mattia Barbarino
Italian Aerospace Research Centre (CIRA), Capua, Italy
e-mail: g.fasulo@cira.it; m.barbarino@cira.it

Oskar Ekblad
PowerCell Group, Gothenburg, Sweden
e-mail: oskar.ekblad@powercellgroup.com

Kristin B. Zimmerman, PhD (eds.), *Dynamic Evironments and Durability Testing, 2026, Vol. 7*, Conference Proceedings of the Society for Experimental Mechanics Series, https://doi.org/10.1007/978-8-743-81446-7_11

Introduction

Hydrogen-Powered Aviation: Challenges and Opportunities

The aviation industry is undergoing a transformative shift toward sustainable propulsion systems, driven by the urgent need to reduce greenhouse gas emissions and achieve carbon neutrality. Among the emerging technologies, hydrogen-powered engines and fuel cell systems represent promising alternatives to conventional jet fuel propulsion. Hydrogen fuel cells offer several compelling advantages for aviation applications, including zero local emissions (producing only water vapor), high energy efficiency, and the potential for quiet operation. Additionally, hydrogen can be produced from renewable energy sources, making it a truly sustainable fuel option.

However, the integration of hydrogen fuel cell systems into aircraft presents significant technical challenges. These include the need for specialized storage systems to handle hydrogen's low volumetric energy density, thermal management requirements, and the necessity to ensure system reliability and safety under the demanding operational conditions of aviation environments. Furthermore, fuel cell stacks must demonstrate exceptional durability and vibration immunity to withstand the dynamic loads encountered during flight operations, including engine vibrations, turbulence, and landing impacts.

The NEWBORN Project Framework

The research presented in this paper was conducted within the framework of the NEWBORN project (NExt generation high poWer fuel cells for airBORNe applications) [1, 2], a European initiative aimed at developing hydrogen-electric propulsion systems for sustainable aviation. The NEWBORN project addresses the critical technological gaps in hydrogen fuel cell integration for aircraft applications, focusing on system optimization, safety, and certification requirements.

Paper Scope and Objectives

This paper describes the vibration analysis activities carried out as part of a specific task within the NEWBORN project, focusing on a fuel cell stack prototype developed by the PowerCell Group [3]. The stack tested and modeled in this work is not the NEWBORN 300-kW stack, but a previous model. The ultimate objective of this research is to conduct a comprehensive vibration immunity analysis of the fuel cell stack to ensure its compliance with aviation standards and operational requirements.

The vibration immunity assessment follows the rigorous requirements outlined in the RTCA document DO-160G "Environmental Conditions and Test Procedures for Airborne Equipment," Section 8 Vibration [4], which establishes the standard testing procedures for airborne equipment certification. Prior to conducting the full durability test procedure, a numerical immunity analysis must be performed to identify critical systems and components requiring detailed examination. This numerical analysis employs stress analysis methods for low to medium-frequency ranges and energy-based approaches for high-frequency evaluation.

The specific scope of the work presented in this paper encompasses preliminary experimental testing of the fuel cell stack, which is designed to address two primary objectives. First, the testing aims to identify potential criticalities in both the fuel cell components and the experimental testing setup at an early stage of the development process. Second, a comprehensive modal survey [5] is conducted to experimentally determine the natural frequencies, damping ratios, and mode shapes of the fuel cell stack. The results of this modal survey serve as the foundation for updating and validating the finite element model (FEM) of the stack, ensuring an accurate representation of its dynamic behavior.

A critical aspect of this work addresses the challenge of boundary condition representation in experimental modal analysis. While correlation between experimental and numerical results is typically performed under known and comparable boundary conditions, assuming a fixed-base condition (clamped at the base) for the fuel cell stack, this assumption may not accurately reflect the actual test conditions. The dynamic coupling between the shaker table and the device under test can significantly influence the measured response characteristics. Therefore, this paper also explores methodologies to correct the experimental data and extract the true fixed-base dynamic characteristics of the fuel cell stack, accounting for fixture coupling effects.

The paper is structured as follows: Section Shaker testing provides a detailed description of the experimental testing setups and procedures employed in this study. Section Experimental modal analysis presents the analysis of experimental data and the comprehensive modal analysis results. Section Finite element model updating introduces the finite element model of the fuel cell stack and describes the model updating process based on experimental findings. Section Fixture coupling neutralization addresses the decoupling analysis methodology for separating the fuel cell dynamics from the slip table effects. Finally, conclusions and recommendations for future work are presented in Section Conclusions.

Shaker testing

This section describes the two different experimental setups employed for the vibration testing of the PowerCell Group fuel cell stack. The testing was conducted using two distinct shaker configurations: the CUBE system and a slip table configuration, as illustrated in Figures 1a and 1b, respectively.

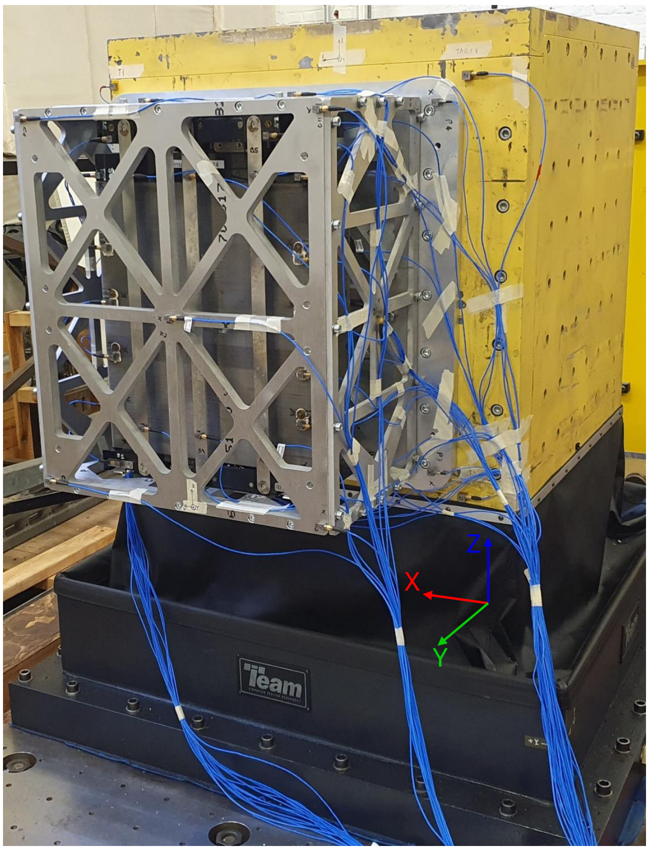

(a) The CUBE multi-axis shaker table [6].

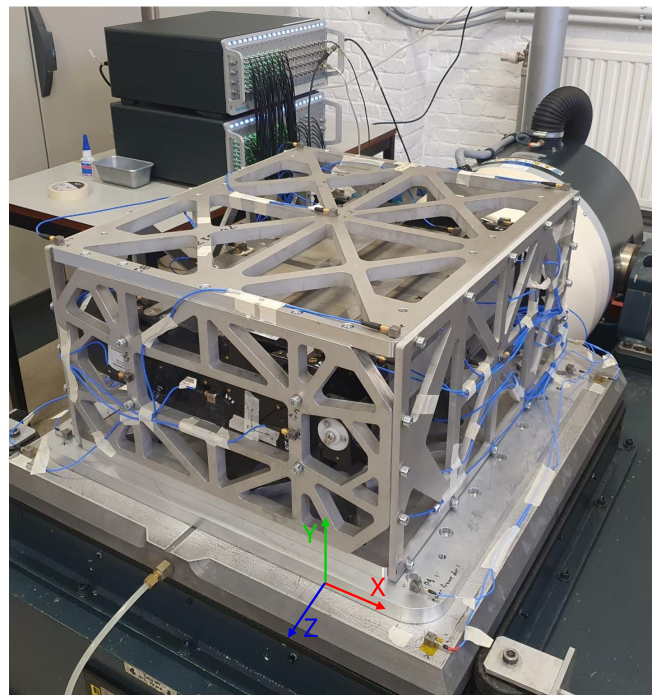

(b) Single-axis slip table.

Fig. 1 Fuel-cell stack shaker table configurations.

In both configurations, the fuel cell stack is securely clamped to the respective testing table through an identical fixture plate. However, the bolt positions are adapted to accommodate the different hole patterns of each table, a consideration that will be further addressed in Section Fixture coupling neutralization. The structure surrounding the fuel cell stack serves as an additional fixture component, referred to as the "cage" throughout this paper. This cage is specifically designed to maintain the stack in boundary conditions that closely simulate operational conditions and can be considered rigid up to a certain frequency threshold.

The main differences between the CUBE and slip table configurations can be summarized as follows:

- **Excitation capabilities**: The CUBE system provides excitation along 6 independent axes, while the slip table is limited to single-axis excitation.
- **Frequency range**: The CUBE system operates up to 300 Hz, whereas the slip table extends the frequency range up to 1000 Hz.
- **Fixture clamping conditions**: Different mounting configurations are required to accommodate the specific interface requirements of each system.

All experimental tests were performed using two Simcenter SCADAS Lab hardware systems [7] configured in a main/secondary arrangement, coupled with Simcenter Testlab software [8] utilizing both structural dynamics and shock and vibration applications.

The instrumentation setup consists of approximately 54 PCB high-sensitivity triaxial accelerometers strategically mounted on the structure to record the dynamic response, resulting in a total of approximately 162 measurement channels. This extensive sensor array ensures excellent spatial discretization for two primary reasons: first, to capture the complex mode shapes of the fuel cell stack with sufficient detail, and second, to provide adequate data for robust finite element model updating and validation procedures. Figure 2 shows the geometry used in the data analysis, indicating accelerometer locations and labels. The orange plate represents the vibration table, the blue plate represents the fixture, the green component represents the fuel cell stack, and the cage is represented by grey lines.

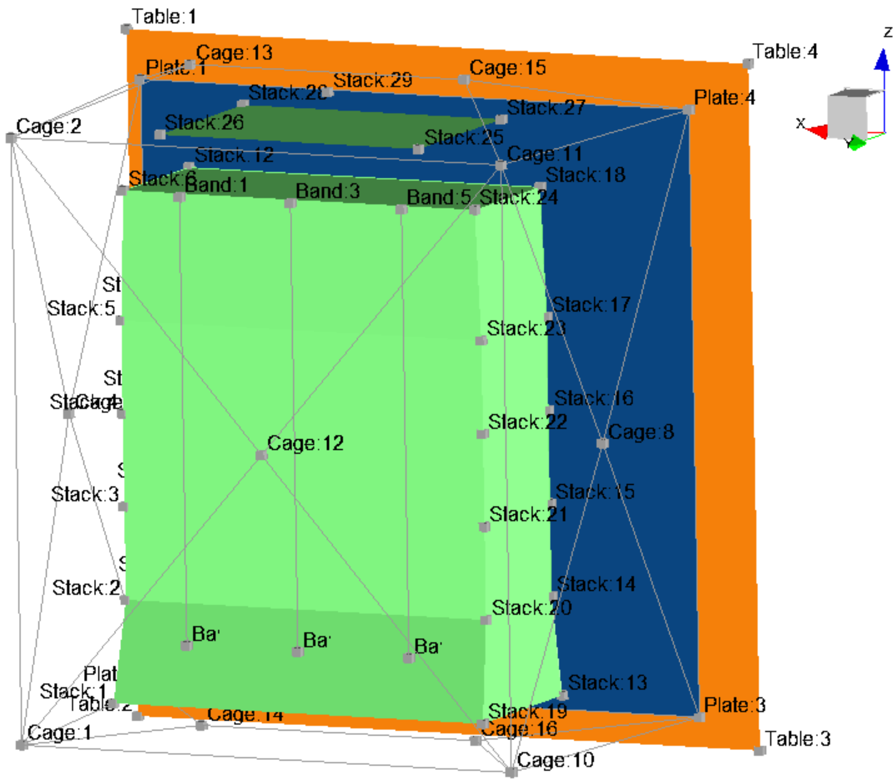

Fig. 2 Test-analysis geometry and sensor locations.

The comprehensive testing program performed on both configurations is summarized in Table 1, which details the various excitation signals, directions, frequency ranges, and excitation levels employed.

Table 1 Summary of vibration tests performed on both shaker configurations

Test	Excitation CUBE	Excitation Slip table	Freq. Range CUBE (Hz)	Freq. Range Slip table (Hz)	Excitation Level
Pseudorandom	X, Y, Z, RX, RY, RZ, XYZ, 6-axis	Z	10–300	10–1000	low, mid, high
Swept sine	X, Y, Z	Z	10–300	10–1000	0.7, 1, 2 (g)

The pseudorandom test refers to an open-loop test with a pseudorandom signal and periodic acquisition, with the parameters in Table 2, using the Simcenter Testlab MIMO FRF application. The Swept sine test refers to a closed-loop test with a logarithmic swept-sine signal with a sweep rate of 1 octave per minute, using the Simcenter Testlab Sine Control application.

Table 2 Open-loop pseudorandom test parameters

Sampling Frequency	Sampling Period	Number of Periods	Number of Realizations
3200Hz	5s	6	5

On the CUBE, for both Sine control and open-loop pseudorandom tests, the excitation level refers to an accelerometer at the top left of the table in Figure 1a, named *Table:1*. More specifically, for the Sine control runs, the defined excitation level of this accelerometer in each direction is controlled, i.e., the software controls the drive to ensure the acceleration follows the target amplitude spectrum; for the open-loop pseudorandom test, this is the resulting excitation level of *Table:1* in the excitation direction of the table. Instead, the accelerometer in *Table:5* placed at the joint between the shaker and table is used for the slip table.

Experimental modal analysis

Although a wide range of tests has been conducted, in this section, we focus only on data from the CUBE. Additionally, only the results in the Z direction are shown. These runs gave the best results in terms of modal excitation and stability in the mode identification.

In all the analyses, the frequency response functions (FRFs) are the transmissibility functions, using *Table:1:+Z* channel as reference.

Figure 3 shows a homogeneity test [9] to understand the degree of nonlinearity of the structure. Some of the most representative points are selected, which together highlight most of the peaks present in the different FRFs. The axis ticks and values are hidden due to confidentiality. Several mode peaks shift with the amplitude of excitation. In particular, most of the modes shift to lower frequency and amplitude with increasing excitation. This is a typical behavior of contact friction nonlinearity [9], which can be due to bolts and cell-to-cell contact. Only one mode, which corresponds to the first bending frequency of the compression bands, increases in amplitude with increasing excitation.

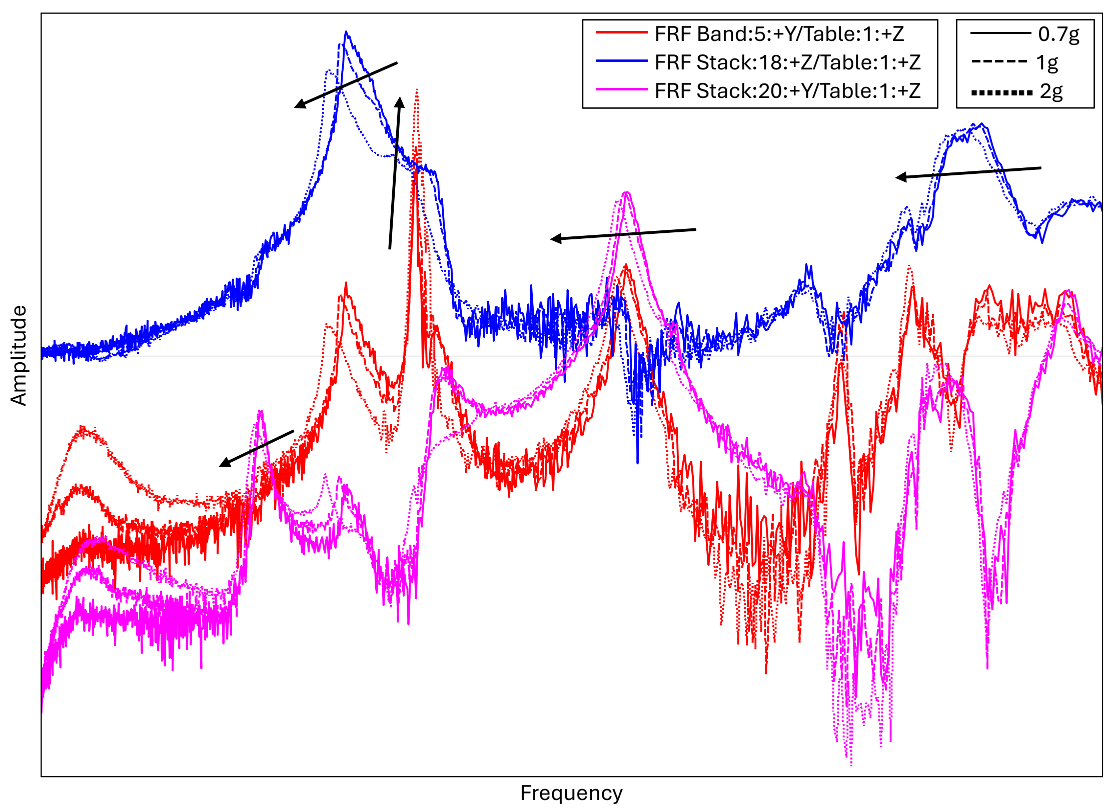

Fig. 3 Homogeneity test of controlled swept sine tests.

Since the goal of the experimental modal analysis is to identify the underlying linear system, open-loop pseudorandom runs are processed, as this type of signal injects less energy at each excited frequency line, and is therefore less prone to excite amplitude-dependent nonlinearities. Indeed, it can be shown that the homogeneity test at three different levels of pseudorandom excitation shows almost overlapping curves.

The data are processed using the Polymax modal parameter estimator [10]. The transfer functions of all the measured channels with respect to *Table:1:+Z* are included in the analysis. The modes are of different types: fuel cell stack body axial mode along Z, bending about X and Y, torsion about Z, and bending of the bands. Most of these modes are identified up to their second order (e.g., second bending, second torsion). Some of the identified mode shapes are plotted in Figure 4. The colored geometry represents the modal deformation, while the grey lines and grey node markers represent the undeformed geometry.

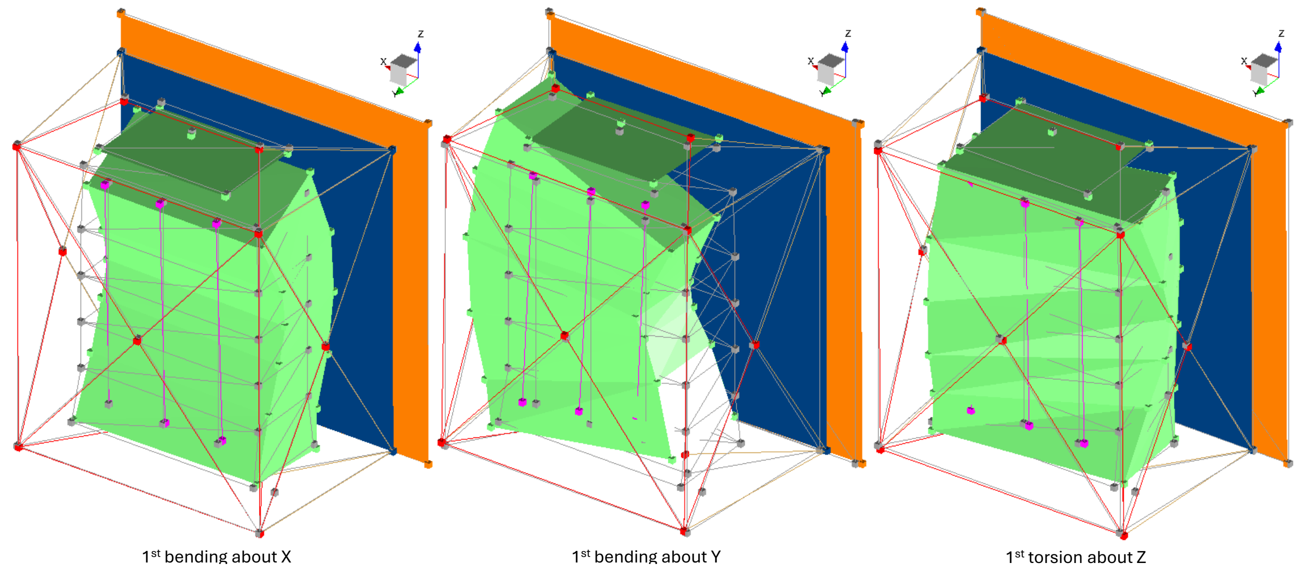

Fig. 4 Identified mode shapes.

The auto MAC (modal assurance criterion) [11] in Figure 5 shows a high degree of discretization between the different modes, as the out-of-diagonal values are very low. The modes increase in frequency from the top left to the bottom right of the matrix. The high values of out-of-diagonal auto MAC, up to 50%, are due to a correlation between flexible modes of the stack and modes due to coupling between the stack and the cage. Indeed, the cage is not rigid in the highest part of the excited frequency band. Instead, the first mode, which slightly correlates with two other modes, is a pseudo-rigid mode of the table, i.e., a rigid rotation of the entire structure, device under test (DUT), and table, about the X axis.

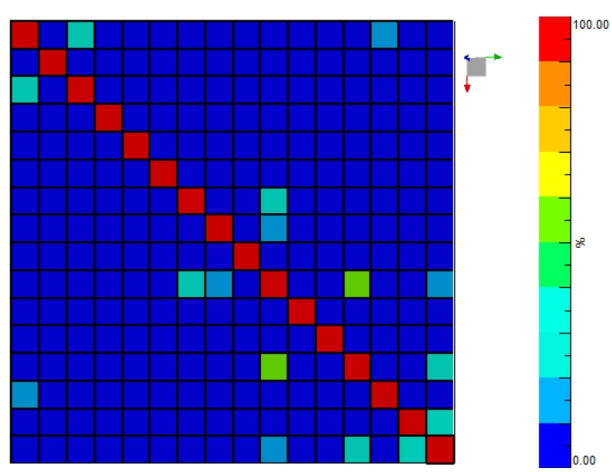

Fig. 5 Auto MAC matrix showing modal correlation.

Figure 6 shows, for three representative points, the modal synthesis of the identified modeset, i.e., a comparison between the measured FRFs and the FRFs synthesized using the modal model. A very accurate modal synthesis is proven, with a level of correlation above 90% for most of the relevant measurement channels.

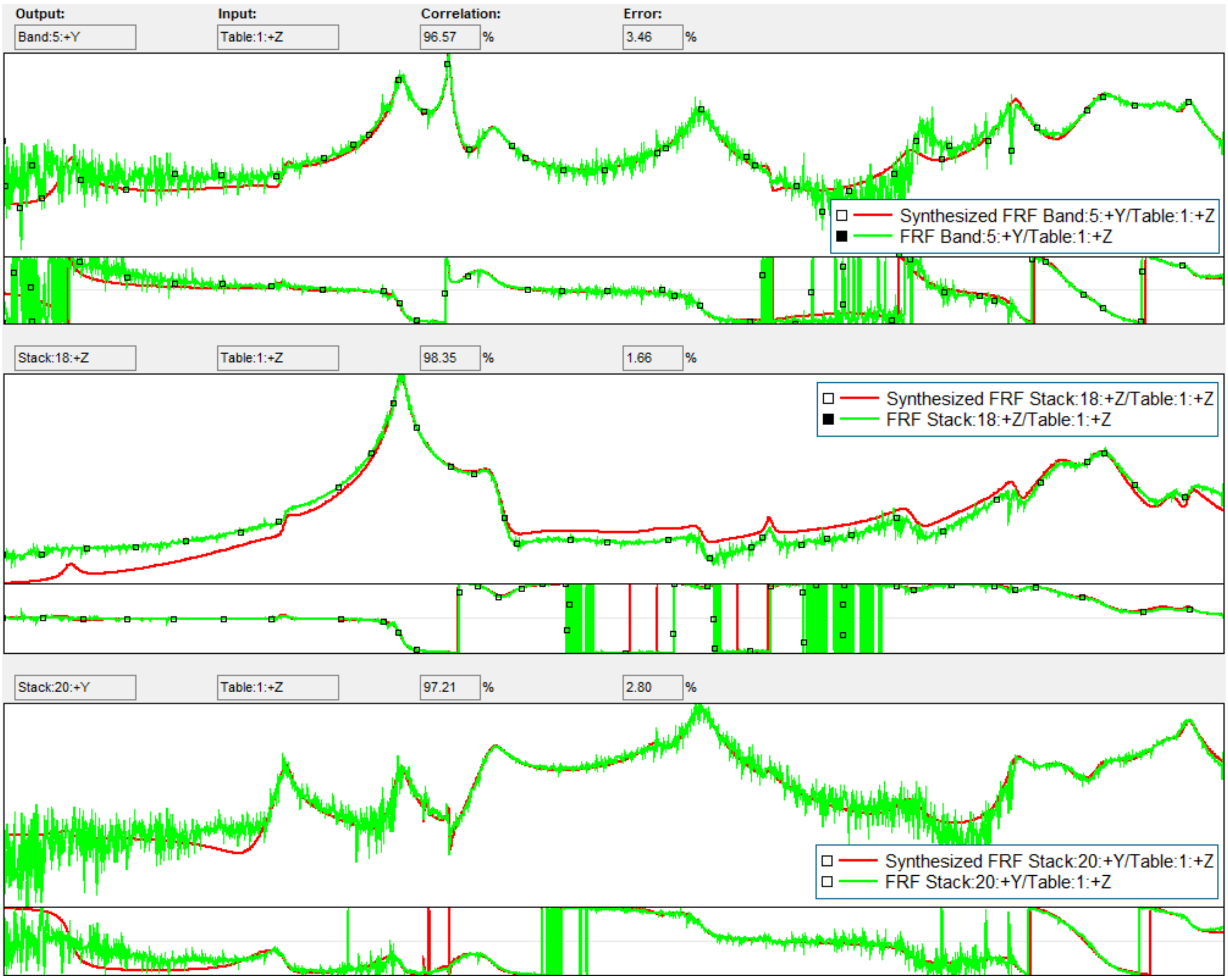

Fig. 6 Modal synthesis validation.

A low level of complexity of the modes is also verified, resulting in a mode phase collinearity above 90% for all the modes.
To summarize, auto MAC, modal synthesis, and mode complexity are the most important indicators for the validation of a modeset. Therefore, the identified modeset can be considered as an accurate test reference for finite element model updating.

Finite element model updating

The FE model of the stack must be used to perform a numerical immunity analysis. To retrieve meaningful information, the FEM must be well correlated with the structure [12]. The model, therefore, requires updating and validation using results from a test reference analysis. In this section, the model is briefly presented, and the results of the model updating are shown. A detailed description of the FEM, including the modeling of the different components in relation to the design inputs and correlation results, can be found in [13]. Instead, this section primarily focuses on the model update from experimental data.

The model updating is performed using Simcenter Nastran SOL200 [14, 15] in Simcenter 3D [16]. The advantage of using Simcenter 3D is that the test reference can be easily imported and correlated with the numerical solution. In particular, the test geometry can be easily aligned with the mesh, and the numerical and test modes are automatically paired based on their MAC and frequency distance. The correlation based on MAC and frequency error is calculated and used as a metric in the optimization function for model updating.

The procedure is as follows:

1. The design variables are defined. These can be either material or element properties. In this case, the assigned design variables are:
    - The Young's modulus of an isotropic material,
    - The six shear moduli of anisotropic materials,
    - The six stiffnesses of spring elements.
2. The design variable definition includes assigning lower and upper bounds. Smaller bounds are assigned to well-known materials, while larger bounds are given to equivalent elements representing a simplification of actual components.
3. The targets are assigned.
4. The errors are calculated.
5. The model update process is performed.
6. The optimized design variables are updated in the FEM.

The last three steps are iterative, as the sensitivities to the design variables are calculated around the initial values. For more details, see [14].

The FEM of the stack includes the cage but does not include the fixture or the shaker table. All the nodes of the face of the cage oriented toward the fixture are clamped.

Figure 7 shows the MAC between the experimentally identified modes and the numerical modes before and after the updating.

Figure 8 shows the test-numerical frequency error: each point represents a pair of numerical and test mode frequencies. The pairing between the modes is automatically computed as in the model update, selecting for each reference (test) mode the numerical mode with the highest MAC value (with a threshold of 0.5). The zero-error line is indicated together with the $\pm 5\%$ bounds, which represent a very acceptable error value.

Figure 8 should be analyzed in combination with Figure 7. The model before updating exhibits relatively low accuracy. Only the first mode pair achieves a frequency error below 5% and displays a comparatively high MAC of about 80%. The second mode pair also demonstrates acceptable correlation. However, all other mode pairs show poor correlation in either frequency or MAC, or both indicators. Additionally, several reference modes do not find a corresponding numerical mode.

In contrast, the model after updating shows excellent agreement in both frequency and mode shape. Most mode pairs achieve errors lower than, or very close to, 5%. All pairs except one present MAC values above 76%, with several exceeding 90%. This is a remarkable result given that 54 triaxial sensors were used for the MAC calculation. The third mode pair, with a MAC value of 63%, corresponds to one of the three bending modes of the compression bands; the other two are not displayed in the MAC matrix plot. In the FEM, these modes involve all three bands equally but with varying phase relationships. In the actual structure, due to asymmetries from band weldings, these modes are slightly split, and each is dominated by the motion of a different band. This structural feature explains the higher error observed in the MAC for this mode, and it is not modeled by choice. The reason for the absence of pairing between the seventh test mode in the MAC matrix and any numerical mode remains unclear. The last four modes are high-order modes with complex shapes that are not captured by the model, as is generally expected.

A comparison between the numerical and experimental calculations of the stack's first bending mode is shown in Figure 9, showing a perfect agreement and the absence of any point of critical discrepancy.

The springs whose stiffnesses were updated correspond to elements that simulate the connection between the compression plate and the top-end plate of the stack, which are located at the top in the representations of the stack. In the initial design, these components were considered to possess flexibility exclusively in the axial (Z) direction. However, experimental analysis revealed significant rotational motion, particularly about the X axis. By including the stiffness of these springs as parameters in the updating process, it was possible to achieve a substantial improvement in both quantitative (MAC) and qualitative (visual inspection) agreement between experimental and numerical mode shapes (Figure 9). This finding underscores the critical importance of validating and, if necessary, refining model assumptions using experimental data [12]. Figure 10 further substantiates this conclusion by visually illustrating the effect of updating the spring elements, through a comparison of the first bending mode before and after the model update.

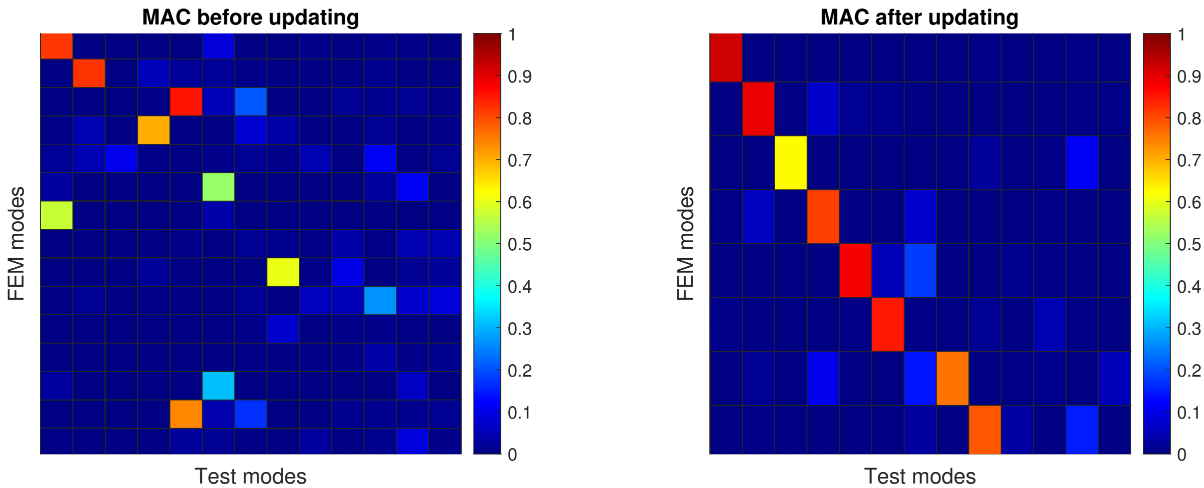

(a) MAC before updating (b) MAC after updating

Fig. 7 Modal Assurance Criterion (MAC) before and after model updating

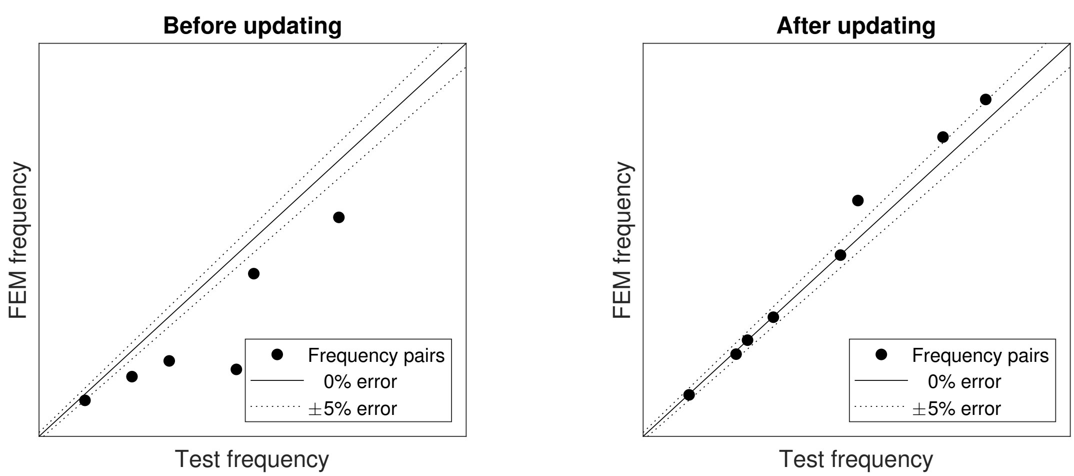

(a) Frequency error before updating (b) Frequency error after updating

Fig. 8 Frequency error between experimental and numerical modes before and after model updating

Fixture coupling neutralization

Introduction to the problem

Aerospace structures are commonly tested on shaker tables for qualification. Typically, a modal survey is conducted separately from qualification tests. Extracting modal parameters directly from the data collected during shaker tests is highly desirable [17, 18, 19, 20], since it offers several advantages, such as:

- Time and cost savings.
- Good modal excitation, especially with multi-axial platforms.
- Increased safety, by reducing handling and transportation between different testing facilities, and avoiding local excitation methods such as modal hammer or secondary shakers.
- Avoidance of overtesting by notching resonances identified as caused by coupling. Indeed, if additional resonances originate from coupling, these can often be notched during qualification tests.

However, the interface between the structure and the shaker introduces fixture coupling effects, which can influence the identification of modal parameters [21, 22]. These effects often result in:

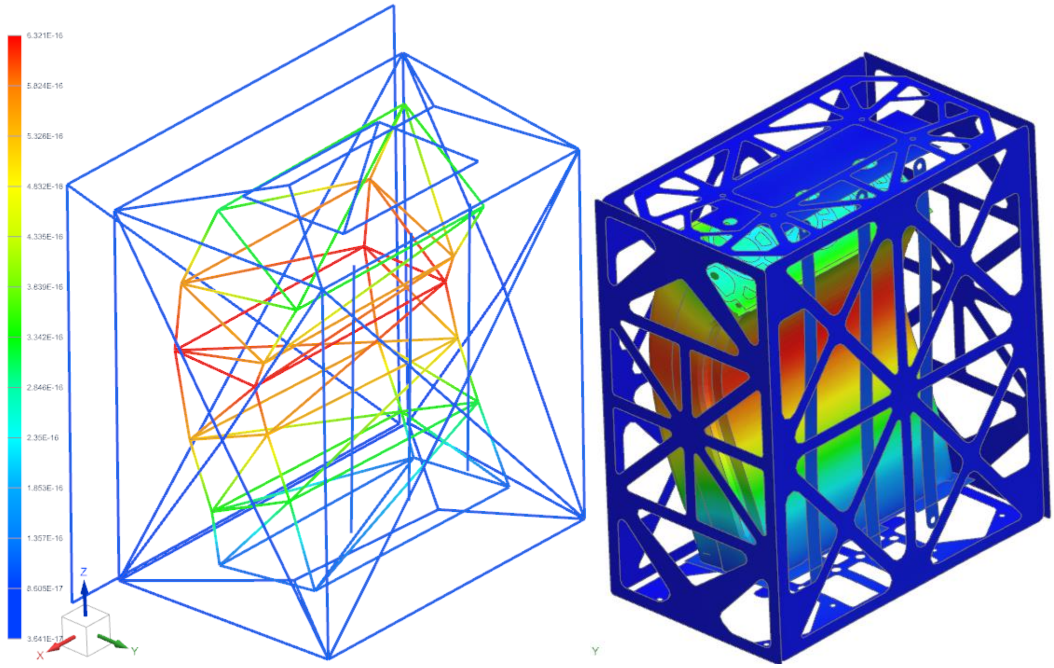

Fig. 9 Comparison of the first bending mode of the stack: numerical vs experimental

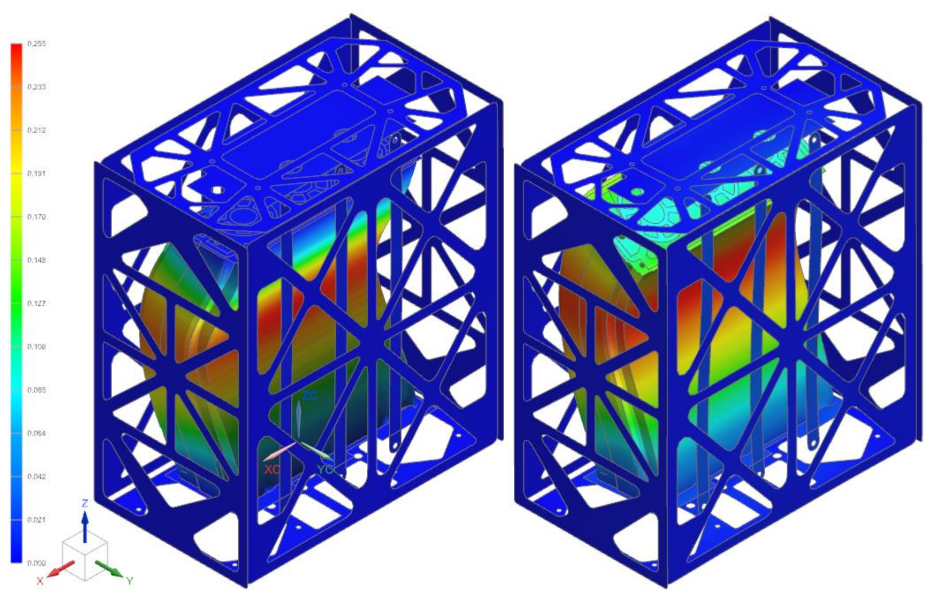

Fig. 10 Comparison of the first bending mode of the stack: before (left) and after (right) updating

- Additional resonances associated with the dynamics of the fixture.
- Modification of the structure's dynamics in terms of mode shapes, natural frequencies, and damping ratios.

The ability to accurately estimate fixed-base (FB) modal parameters is essential for model correlation, as shown in the previous section, as well as for structural response prediction and qualification processes. Constraining a model with non-trivial boundary conditions, such as fixed-base or free boundaries, introduces further challenges that should be avoided. The goal of fixture coupling neutralization is therefore to correct the coupled dynamics to recover the characteristics of the device under test (DUT).

Various decoupling methodologies have been developed in the literature. Early approaches utilize transmissibility-based methods [21, 22], while others employ multi-axial excitation and direct force measurements at the interface [17, 18, 19, 20].

More recent methods provide solutions for reconstructing FB modes from coupled data, such as [23, 24, 25, 26, 27] and [28, 29, 30, 31, 32, 33, 27]. These strategies allow for more accurate identification of the structure's inherent dynamic properties.

A schematic representing the coupling effects due to table flexibility or pseudo-rigid table modes is shown in Figure 11, together with the goal of decoupling.

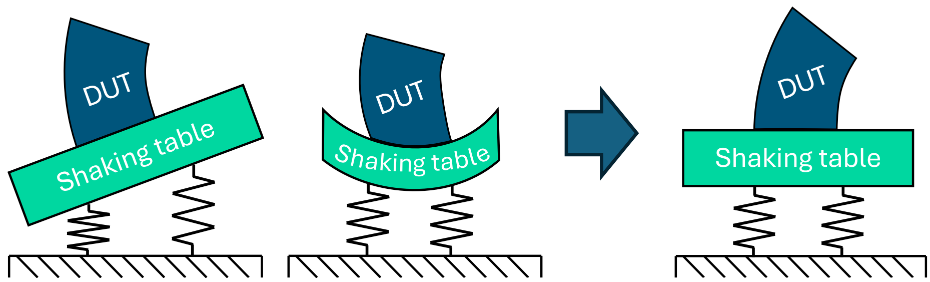

Fig. 11 Visual explanation of coupling and decoupling effects.

Employed methodologies

In this paper, the approaches presented in [23, 34, 35] by the same main author, Randy L. Mayes, are explored, namely the Frequency-based approach [23], the Modal-based approach [34], and the Singular value decomposition based approach [35]. The methods in [28, 36, 29, 30, 31, 32, 37, 33, 27] were not used, since only one direction of excitation was available, while several constraint modes were observed.

Frequency-based approach

To summarize this approach:

- The FB boundary conditions are mathematically constrained.
- An estimation of the shaker force is required.
- The full FRF matrix must be synthesized.
- The classical mathematical constraints used to produce FB conditions are modified to mitigate the ill-conditioning that typically arises when employing conventional constraint equations.

The mathematical basis, and the testing and analysis procedures in [23], are reported here for completeness. The input-output equation can be partitioned as follows:

$$\left\{ \begin{array}{c} \mathbf{a}_f \\ \mathbf{a}_c \end{array} \right\} = \left[\begin{array}{cc} \mathbf{H}_{ff} & \mathbf{H}_{fc} \\ \mathbf{H}_{cf} & \mathbf{H}_{cc} \end{array} \right] \left\{ \begin{array}{c} \mathbf{f}_f \\ \mathbf{f}_c \end{array} \right\}, \tag{1}$$

where $\mathbf{a}$ and $\mathbf{f}$ are vectors of acceleration and force, respectively, $\mathbf{H}$ is an FRF matrix, subscript c refers to the degrees of freedom (DOFs) to be constrained, and subscript f to the free ones. Only a few columns, or sometimes just one column, of this matrix are measured. Therefore, the first step is to reconstruct the entire matrix using the modal parameters extracted from the measured columns. By setting the corresponding constrained DOFs to zero (i.e., $\mathbf{a}_c = \mathbf{0}$), Equation 1 can be reformulated as shown in Equation 2.

$$\mathbf{a}_f = \left[\mathbf{H}_{ff} - \mathbf{H}_{fc}\mathbf{H}_{cc}^{-1}\mathbf{H}_{cf}\right]\mathbf{f}_f \tag{2}$$

As $\mathbf{H}_{cc}^{-1}$ is often poorly conditioned, the physically constrained DOFs are reduced to the modal coordinates of the table, using its modal matrix $\mathbf{\Phi}_c$, to enhance stability. The final form of the correction is given in Equation 3.

$$\mathbf{a}_f = \left[\mathbf{H}_{ff} - \mathbf{H}_{fc}\mathbf{\Phi}_c^{T+}\left(\mathbf{\Phi}_c^{+}\mathbf{H}_{cc}\mathbf{\Phi}_c^{T+}\right)^{-1}\mathbf{\Phi}_c^{+}\mathbf{H}_{cf}\right]\mathbf{f}_f \tag{3}$$

This modification significantly improves the robustness of the results. The procedure for obtaining FB FRFs can be summarized in the following steps:

1. The mode shapes of the bare table can be identified either by performing a modal shaker test or by using a modal hammer.

2. The Device Under Test is mounted on the shaker table, and two tests are performed:

   - An external shaker is attached to the tip of the table with a force gauge. The acceleration due to this force at the shaker location is measured. A modal hammer can also be used. The output of this test is $\mathbf{H}_{st}$.
   - The tip-shaker is removed and a shaker table test is performed to obtain the transmissibility to tip accelerations $\mathbf{a}_i/\mathbf{a}_t$.

   The additional shaker test is performed to estimate the shaker force using Maxwell's reciprocity principle. This estimation is necessary because the next step (synthesizing the FRF matrix) requires calculation of the modal mass, which requires a driving point FRF. However, the input force at the shaker is typically not measured. To circumvent this, the following procedure is applied:

   - The relationship between the FRFs is: $\mathbf{H}_{st} = \mathbf{H}_{ts}$
   - The acceleration at the tip of the table is: $\mathbf{a}_t = \mathbf{H}_{st}\mathbf{f}_s$
   - Rearranging for the shaker force: $\mathbf{f}_s = \mathbf{a}_t/\mathbf{H}_{ts}$
   - Substituting: $\mathbf{f}_s = \mathbf{a}_t/\mathbf{H}_{st}$
   - The FRF at any location of interest is then: $\mathbf{H}_{is} = \mathbf{a}_i/\mathbf{f}_s$
   - Finally, substituting the acceleration, the accelerance FRF is estimated as: $\mathbf{H}_{is} = \mathbf{H}_{st}\mathbf{a}_i/\mathbf{a}_t$

3. Extract modal parameters from the accelerance FRFs.

4. Synthesize the full FRF matrix using the modal parameters obtained in the previous step. This is a critical step, and can be quickly performed in Testlab [8] if a driving point FRF is available. However, the synthesis of FRFs for the additional input columns is not always accurate. The accuracy in this step plays an important role in the final estimation of the fixed-base characteristics.

5. Apply the constraint Equation 3 to the synthesized FRFs.

The fixed-base FRFs are therefore obtained and can be used for modal analysis.

Modal-based approach

The approach in [34] enables the structural system to be constrained solely through the modal shapes of the assembly, the structure under test, and the table, along with the modal shapes of the bare table. To ensure clarity, the following nomenclature is adopted:

- $\mathbf{\Phi}_c$: modes of the table alone,
- $\mathbf{\Psi}$: modes of the assembly (structure and table combined),
- $\mathbf{\Psi}_c$: assembly modes associated exclusively with the DOFs of the table.

Again, the theory in [34] is reported for completeness. The first step is to define the $\mathbf{B}$ matrix as the projection of $\mathbf{\Psi}_c$ onto $\mathbf{\Phi}_c$, as shown in Equation 4.

$$\mathbf{B} = \mathrm{pinv}(\mathbf{\Phi_c}) \cdot \mathbf{\Psi}_c \tag{4}$$

The matrix $\mathbf{B}$ provides, through its coefficients, a measure of the contribution of each mode in $\mathbf{\Psi}_c$ to the modes of $\mathbf{\Phi}_c$. By exploiting orthogonality, the non-zero coefficients in Φ_c correspond to modes in $\mathbf{\Psi}_c$ that are similar to those in $\mathbf{\Phi}_c$. Thus, in essence, $\mathbf{B}$ defines the constraints that establish the clamping of the base. Subsequently, the null space of $\mathbf{B}$ can be computed as in Equation 5, and this gives the directions of $\mathbf{\Psi}_c$ not captured by $\mathbf{\Phi}_c$.

$$\mathbf{L} = \mathrm{null}(\mathbf{B}) \tag{5}$$

This represents a coordinate transformation, which enables reducing the number of free modal coordinates to a smaller, constrained set. By applying $\mathbf{L}$ and solving the eigenvalue problem, the FB natural frequencies ω_{fix} and the corresponding eigenvectors $\mathbf{\Gamma}$, which should be mass-normalised, are obtained. The eigenvalue problem to be solved is given in Equation 6, which is formulated under the assumption of unit-mass scaled modal shapes and with the damping matrix $\mathbf{C}$ neglected.

$$\left[\mathbf{L}^T \operatorname{diag}(\omega_{\text{ass}}^2)\mathbf{L} - \omega^2 \mathbf{L}^T \mathbf{I} \mathbf{L}\right] q = 0 \tag{6}$$

When accounting for damping, the formulation is modified as in Equation 7.

$$\left[\omega^2 \mathbf{L}^T I \mathbf{L} - \omega \mathbf{L}^T 2\, \zeta_{\text{ass}} \omega_{\text{ass}} \mathbf{L} + \mathbf{L}^T \operatorname{diag}(\omega_{ass}^2)\mathbf{L}\right] q = 0 \tag{7}$$

Finally, it is necessary to return to physical coordinates. The FB mode shapes are then computed as in Equation 8, following the formulation in [34].

$$\mathbf{\Psi}_{\text{fixed}} = \mathbf{\Psi} \mathbf{L} \mathbf{\Gamma} \tag{8}$$

Singular value decomposition based approach

A valid alternative to avoid characterizing the bare table is presented in [35]. Singular Value Decomposition (SVD) is applied to the assembly modal shapes, considering only the boundary DOFs as in Equation 9.

$$\mathbf{USV}^H = \mathbf{\Psi_c} \tag{9}$$

Then $\mathbf{U}$ is used to modify $\mathbf{\Psi_c}$ as shown in Equation 10.

$$\mathbf{T_{ref}} = \mathbf{U\Psi_c} \tag{10}$$

$\mathbf{T_{ref}}$ is then used in Equation 4 instead of $\mathbf{\Phi_c}$. However, only a few columns, i.e., a limited number of modes of $\mathbf{T_{ref}}$, should be included in the correction to avoid over-decoupling the dynamics.

This method has proven effective in constraining the boundary, removing the table modes, and correcting the FB frequencies and modal shapes. Additionally, no bare table characterization is required.

Comparison of approaches

Table 3 summarizes the differences among the methods, outlining their respective requirements and limitations.

Table 3 Comparison of method requirements and limitations.

Frequency based	**Modal based**	**SVD based**
$a_f = [H_{ff} - H_{fc}\, \Phi_c^{T+} (\Phi_c^+ H_{cc} \Phi_c^{T+})^{-1} \Phi_c^+ H_{cf}] f_f$	$\Psi_{\text{fixed}} = \Psi \mathbf{L} \Gamma$	$[U][S][V]^H = \Psi_c$
Synthesize full FRF matrix, and conduct a separate bare table test.	Separate bare table test for modal shapes.	No modal test for bare table required.
Sensitive to synthesized FRF accuracy.	Unit mass scaling needs driving point FRF.	Unit mass scaling needs driving point FRF.

To avoid constraining the test article modes but only constraining the table modes, a guiding rule for choosing the number of shapes in Φ_c exists [35]. Specifically, the number of modes dominated by the shaker table dynamics, when testing the test article on the table, must be at least equal to the number of constraint shapes in Φ_c.

Fixture decoupling results

Here, the case of the fuel cell stack is analyzed. First, in Evidences of coupling, the investigation shows qualitatively and quantitatively the coupling between the DUT (fuel cell stack and cage) and the shaking table (table and fixture). Secondly, the methodologies described in Employed methodologies are verified to mitigate the effect of the coupling and to extract the fixed-base modes.

Evidences of coupling

Summarizing what is described in Introduction to the problem, the main evidence of coupling is the appearance of additional resonances associated with the dynamics of the fixture and a modification of the modal parameters. This is, of course, due to FRFs not representing fixed-base characteristics. Placing sensors at the boundary conditions (i.e., on the fixture and on the table) allows identification of whether the mode shapes of the DUT involve motion of the boundary DOFs, thereby detecting coupling. If the boundary DOFs are accessible, this verification is always possible. However, a modification of the natural frequencies (for example) can only be detected when a fixed-base reference is available. This is the case for the fuel cell stack. As described in Shaker testing and shown in Figure 1, the stack was mounted and tested on two different shaker tables: the CUBE and a slip table. While the data acquired on the CUBE show relatively low motion of the boundary DOFs, the slip table data show all the aforementioned signs of coupling. The authors believe that this is mainly due to different methods of fixing the fixture. In particular, as shown in Figure 12, the fixture is bolted to the slip table only in the middle, due to alignment between holes. For the CUBE, holes close to the border were used for clamping, providing better clamping and lower fixture motion, which is assumed here to explain the difference in coupling between the two setups. Therefore, in this analysis, the CUBE's mode shapes and frequencies are assumed as the fixed-base reference.

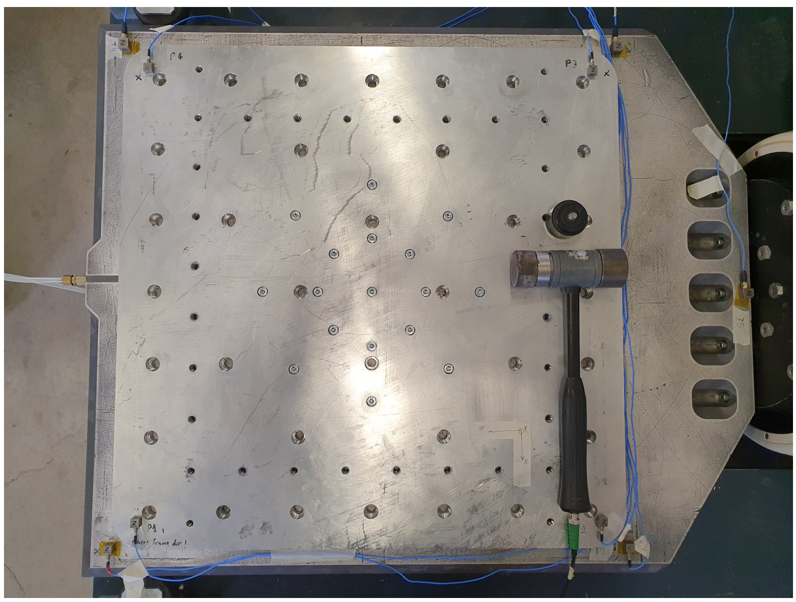

Fig. 12 Slip table to fixture fixing

Figure 13 presents the MAC between the CUBE and slip table modes. A few observations are listed below, together with information about frequencies.

- The slip table modeset has a few more modes in the bandwidth of the stack flexible modes. While CUBE mode 1 is pseudo-rigid, additional modes are present for the slip table, e.g., mode 7. The presented MAC matrix is from a selection of slip table modes that best correlate with the CUBE modes; several stable modes from the stabilization diagram were discarded during the modal validation.

- At lower frequencies, the correlation between the modesets is higher, while at higher frequencies it degrades. This is because:

  - At lower frequencies, the cage is rigid and the DUT couples mainly with fixture and table motion. At higher frequencies, the cage is more flexible and its dynamics couple with those of the fixture.
  - Modes 4, 5, and 6 of the CUBE, or 3, 4, and 5 of the slip table, are the compression band modes, which are local.

- Several slip table modes, even those with high MAC, are shifted down in frequency, indicating more flexible boundary conditions. Denoting CUBE modes as $C1$, $C2$, etc., and slip table modes as $ST1$, $ST2$, etc., some frequency relations are: $ST1$ is 96% of $C2$; $ST2 = 87\%\, C3$; $ST8 = 93\%\, C8$; $ST9 = 90\%\, C9$; $ST14 = 92\%\, C12$.

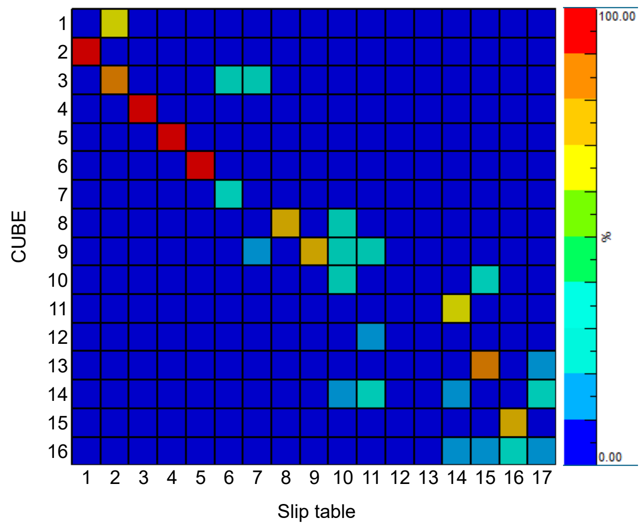

Fig. 13 MAC between CUBE and slip table modes

Figures 15, 16, and 14 present comparisons between pairs of modes shown to be impacted by coupling. In all cases, the eight boundary sensors for the CUBE are almost static, while there is significant motion—especially of the fixture—for the slip table.

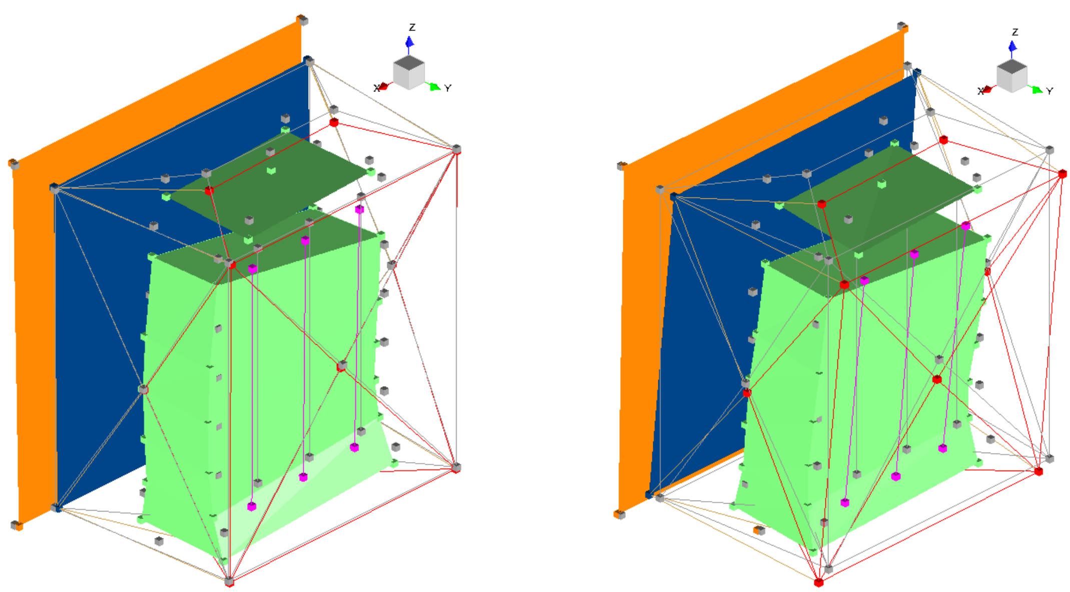

(a) CUBE ($C3$)

(b) Slip table ($ST2$)

Fig. 14 Comparison of 1^{st} longitudinal mode shapes along Z between shaker tables. $ST2 = 87\%C3$.

Decoupling of longitudinal mode

Here, the decoupling of the 1^{st} longitudinal mode shape along Z is investigated, as it is one of the most affected by coupling. As previously reported, for the slip table, the longitudinal mode frequency ($ST2$) is 87% of that of the CUBE setup, and their mode shapes are compared in Figure 14, with a MAC value of 82%. All results are presented using the CUBE's $C3$ mode as reference.

The Frequency-based approach and Modal-based approach require identification of the table's modes, isolated from the DUT. To this end, slip table modes with only the fixture mounted were identified via hammer testing and Polymax postprocessing [10]. The setup is shown in Figure 12.

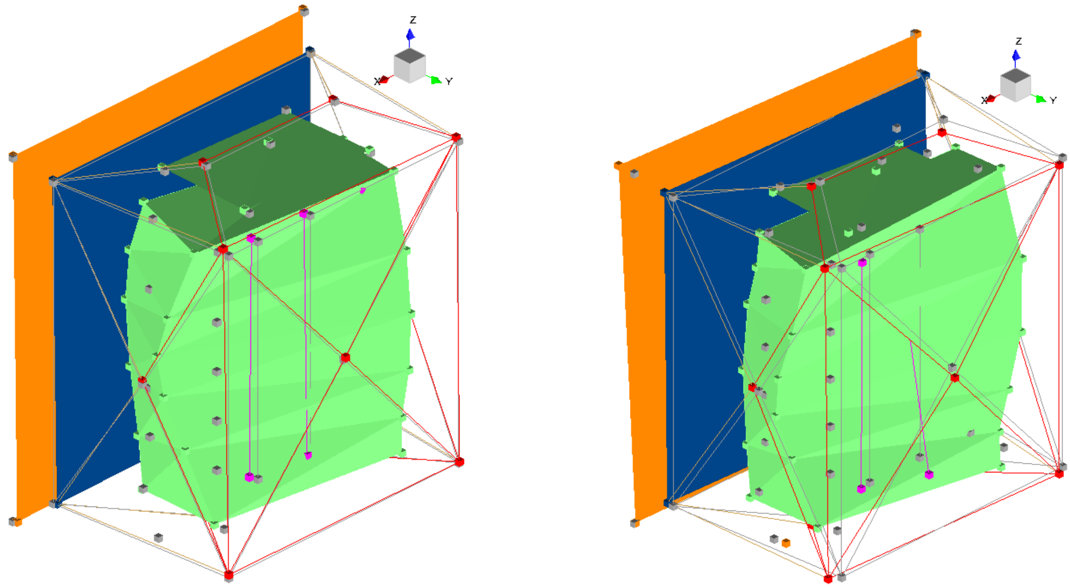

(a) CUBE ($C8$) (b) Slip table ($ST8$)

Fig. 15 Comparison of 1^{st} torsional mode shapes between shaker tables. $ST8 = 93\%C8$.

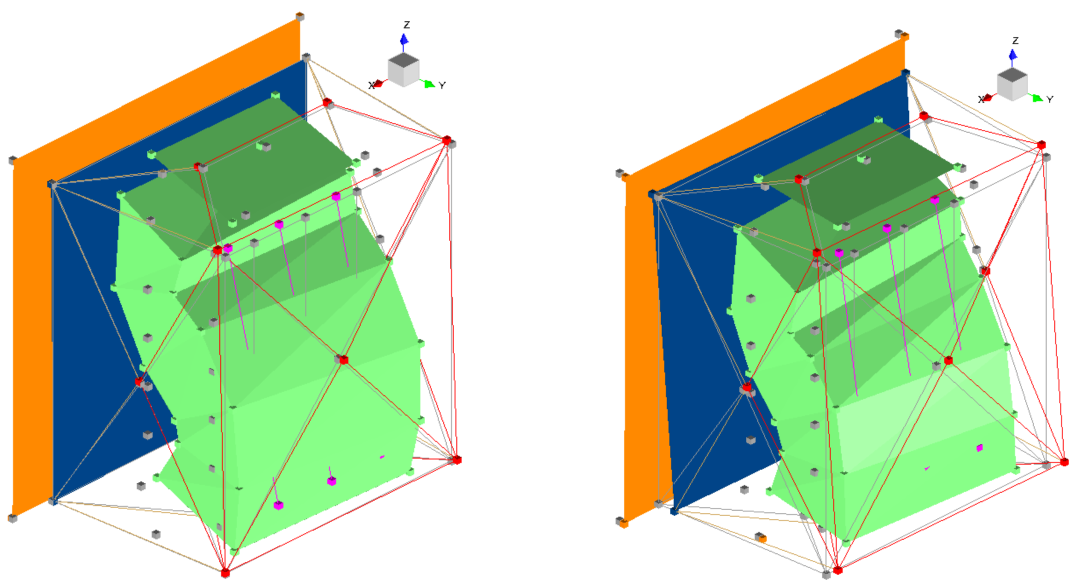

(a) CUBE ($C9$) (b) Slip table ($ST9$)

Fig. 16 Comparison of 2^{nd} bending (about X axis) mode shapes between shaker tables. $ST9 = 90\%C9$.

Selecting all modes in the frequency band of interest would lead to incorrect correction. If the number of table modes used in the correction exceeds the actual number of modes coupled with the structure, the correction can compromise the structural modes themselves [23] because modes not coupled would also be incorrectly adjusted.

Thus, the main challenge in applying this method is accurately identifying the table modes. The mode selection was lengthy, mainly based on correlation with the assembly modes (considering only the table's DOFs) and on trial and error.

Figure 17 shows the selected bare table modes. The fuel cell stack geometry is included as a reference, but the stack was not mounted on the table when identifying those modes. The modes depict the motion of both the table and fixture, as well as their relative movement. This illustrates a complex scenario where different components contribute to the coupling.

The Frequency-based approach is then applied. Not all DOFs have been used for the correction; those related to the compression bands were excluded as they mostly contribute only to their associated modes. By omitting these components,

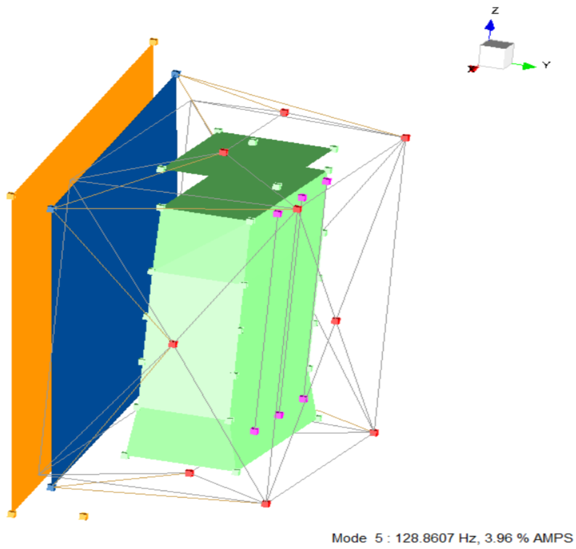

(a) 1^{st} mode: 128 Hz

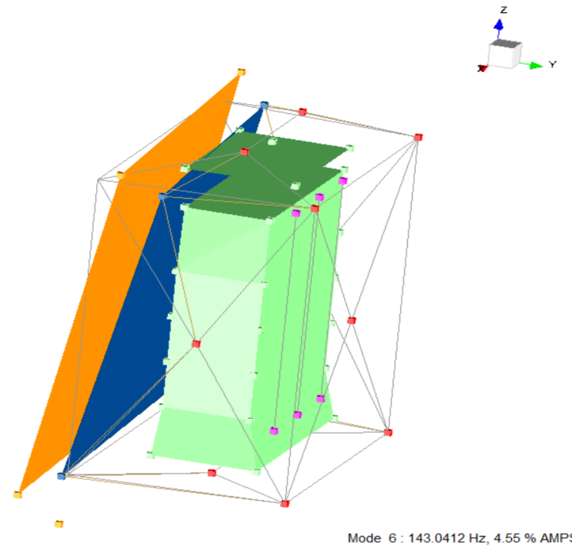

(b) 2^{nd} mode: 143 Hz

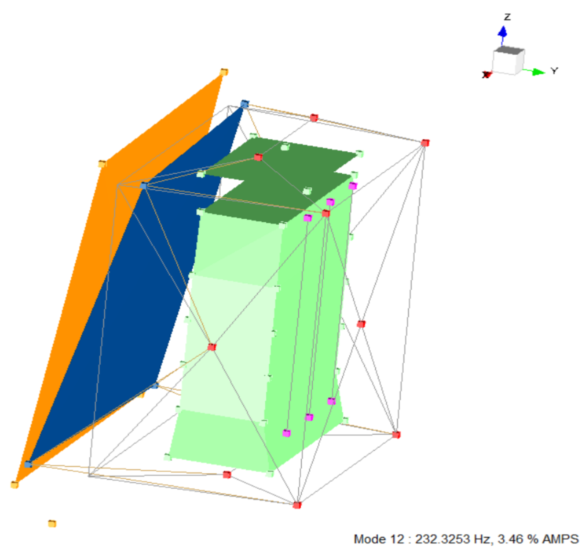

(c) 3^{rd} mode: 232 Hz

Fig. 17 Slip table and fixture modes (without fuel cell stack).

subsequent operations like FRF matrix synthesis—an important step—are simplified, and the correction can be focused on the actual coupled modes. Equation 3 is applied using the modes at 143 Hz and 232 Hz as the table mode matrix $\mathbf{\Phi}_c$. As a result, the additional modes originating from coupling are removed.

The corrected axial mode from the Mayes method is shown in Figure 18. There is still some cage movement, but it is significantly reduced. Despite this, the MAC remains above 80%. The corrected frequency is about 105% of that mode's natural frequency on the CUBE ($C3$), thus the correction changes the error from -13% to $+5\%$, i.e., from 87% to 105% of $C3$. The reason for this frequency overshoot requires further investigation.

The Modal-based approach has also been applied to the same mode. Results, shown in Figure 19, were obtained using three different datasets of table modes, and are summarized in Table 4. This method effectively eliminates the movement of both the fixture and the table. The cage remains stationary, resulting in a better modal shape outcome than that from the Frequency-based approach. All corrected modes show a MAC greater than 80% relative to the CUBE axial mode. However, the frequencies are substantially different from the CUBE reference.

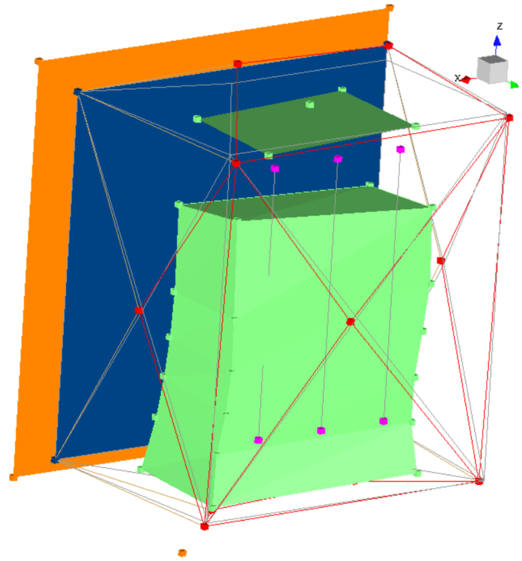

Fig. 18 Corrected FB longitudinal mode obtained with the Frequency-based approach. $ST2 = 105\%C3$

Table 4 Summary of results of Frequency-based approach as a function of selected table shapes.

Bare table modes		
1	2	3
128 Hz 143 Hz	128 Hz 232 Hz	143 Hz 232 Hz
Correction result modal approach		
1	2	3
$126\%C3$	$149\%C3$	$151\%C3$

Another notable aspect is that the modes obtained through the correction show a slight increase in modal complexity. The results are highly sensitive to the table modes used, especially regarding frequency estimation.

Because of the high sensitivity to table mode selection, the Singular value decomposition based approach was also applied, as it avoids the need for bare table modes and appears more effective for frequency correction [35]. The first attempt applied SVD to the $ST2$ mode and used the resulting $\mathbf{U\Psi}_{ST2,c}$ as $\mathbf{\Phi}_c$ to constrain the DOFs. The frequency changed from $87\%C3$ before correction to $99.9\%C3$, very close to the reference, but the correction did not significantly change the modal shape; the fixture still showed motion.

The second attempt applied SVD to the entire assembly matrix (boundary DOFs only), retaining the two dominant singular values. The resulting mode shape (see Figure 20) shows nearly zero cage motion. The MAC value is 88% relative to the CUBE longitudinal mode (higher than the 82% MAC of the slip table longitudinal mode). However, the frequency is $123\%C3$, the best obtained with this approach.

Decoupling of bending and torsion

The same procedure was also attempted for other modes, such as the torsional about Z ($C8$ and $ST8$) and the 2^{nd} bending about X ($C9$ and $ST9$). A thorough study is still required to identify which table modes should be considered for effective correction. The Singular value decomposition based approach was used to avoid manually selecting table modes, relying only on the assembly's modal shape matrix. However, for the torsional mode, results remained inconclusive, suggesting that further investigation is needed.

For the 2^{nd} bending about X, while the SVD method increased mode complexity, the corrected frequency was 98% of $C9$, improving from the original value of $90\%C9$ before the correction. The corrected modal shape is shown in Figure 21.

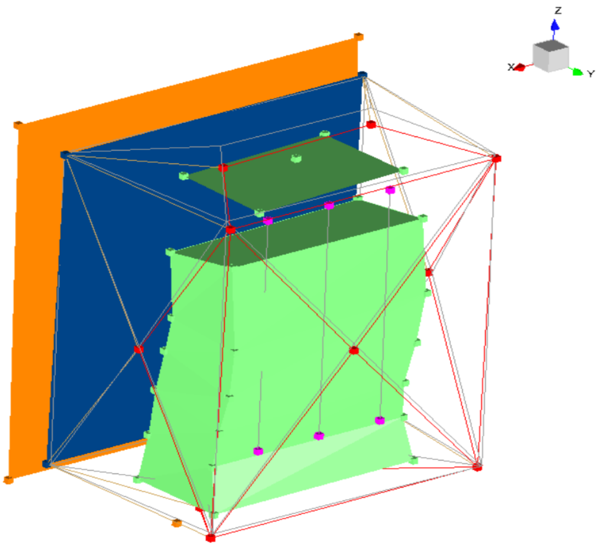

(a) 1^{st} Corrected mode: $127\%C3$

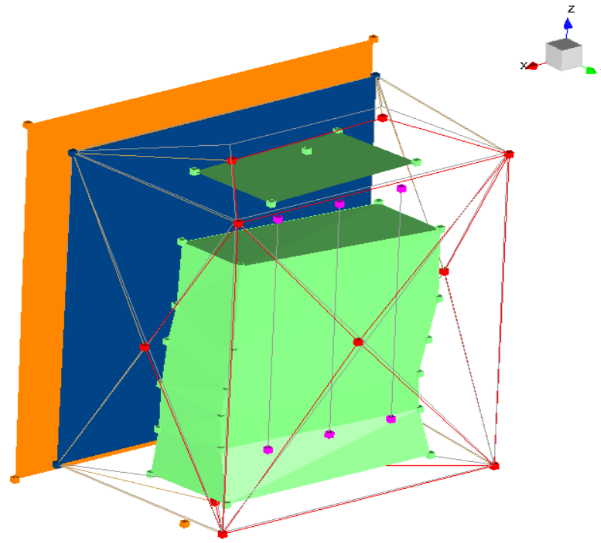

(b) 2^{nd} Corrected mode: $149\%C3$

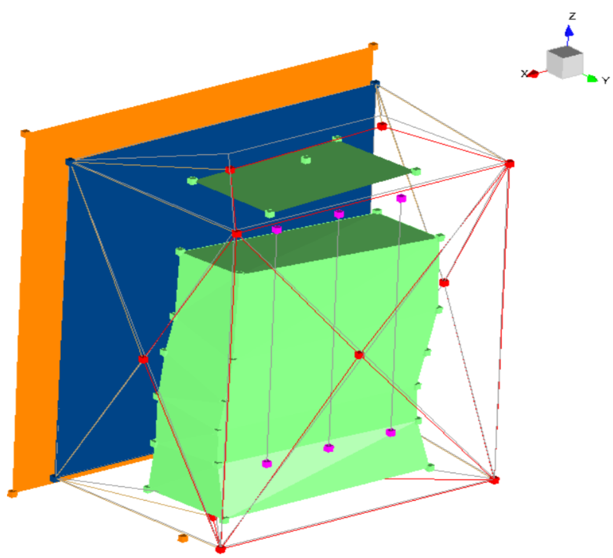

(c) 3^{rd} Corrected mode: $151\%C3$

Fig. 19 Modal shape correction results for the longitudinal mode: Modal-based approach.

Comments and summary of decoupling results

In performing these corrections, the DOFs of the fixture were treated as boundary conditions—taken as a first approximation to be equivalent to those of the cage (i.e., the actual structural component). This was motivated by the observation that, without fixing these DOFs, the correction process did not adequately suppress the fixture's motion, resulting in inaccurate results. This may suggest that the relative motion between the fixture and cage plays a non-negligible role in the dynamics. A more rigorous approach could involve placing additional accelerometers directly on the cage to capture and account for its motion relative to the fixture. Since fixture and cage are bolted together, their interface introduces a further layer of complexity to the system's dynamics, which would benefit from a more comprehensive instrumentation setup.

This preliminary application of the decoupling method focuses on correcting a few of the most coupled modes per time, but the approach has inherent limitations. Correction accuracy depends on proper identification of table modes and precise estimation of coupling effects. Future work could expand the analysis to include all highly coupled modes (longitudinal,

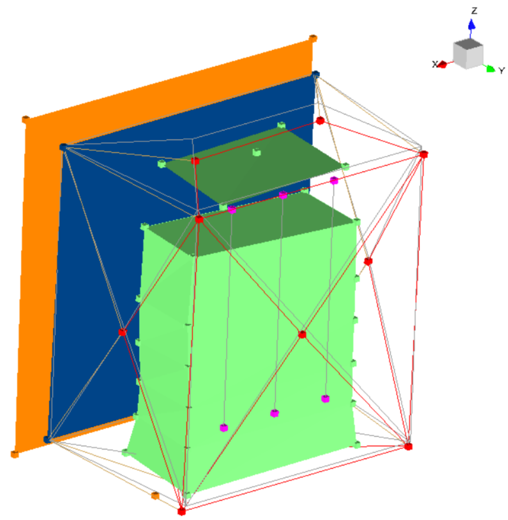

Fig. 20 Longitudinal mode corrected using the Singular value decomposition based approach: $123\%C3$

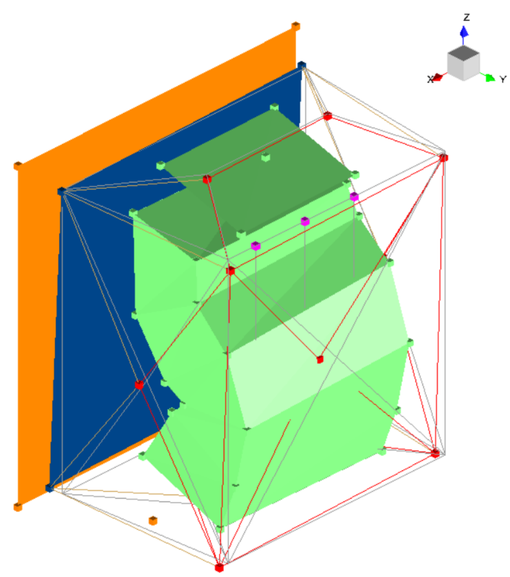

Fig. 21 2^{nd} bending about X, corrected using the Singular value decomposition based approach: $98\%C9$.

torsional, and bending) simultaneously, allowing for a more comprehensive validation and deeper insight into the slip table–structure interaction.

It is important to note that if the table mode shape is directly extracted from the assembly modes—considering only the boundary DOFs of the longitudinal coupled mode—and used for correction, the longitudinal mode may completely disappear. This indicates the method's sensitivity to the proper selection of the correction basis.

Among the three approaches of the method, the Singular value decomposition based approach was able to retrieve the corrected FB modal shape for the longitudinal mode, with a higher MAC value than the shape obtained on the CUBE (used here as reference), although the frequency was not corrected. When the same method was applied using exactly the table's DOFs in the assembly matrix, the frequency obtained was very close to the CUBE value.

The same procedure applied to another coupled mode allowed the method to fix the fixture and achieve a frequency close to the CUBE reference, despite increased mode complexity.

It is important to note that including more columns from $\mathbf{T_{ref}}$ after SVD degrades results and causes loss of information, causing the correction to fail. This is consistent with [35], which reports that including more modes than necessary results in the correction affecting the actual structural modes as well.

Conclusions

This study addressed the dynamic characterization of a fuel cell stack through experimental testing, modal analysis, finite element model (FEM) updating, and fixture coupling neutralization, with a focus on supporting the development and qualification of vibration-robust hydrogen fuel cell systems for aviation.

The main conclusions from each step of the workflow, as well as points of synergy between the activities, are as follows:

- **Shaker Testing and Experimental Modal Analysis:** The thorough experimental campaign, utilizing multiple shaker platforms and a dense array of accelerometers, enabled high-quality data collection for a wide range of excitation conditions. The comprehensive modal survey provided reliable identification of natural frequencies, damping ratios, and mode shapes, while also revealing amplitude-dependent nonlinearities, particularly due to friction. Robust validation of the modal dataset was achieved through auto-MAC assessment, modal synthesis, and complexity analysis, yielding a highly credible experimental modal model.
- **FEM Updating and Test-Analysis Correlation:** The availability of an accurate experimental modal model proved fundamental for the successful updating and validation of the FEM. By directly using the experimental mode shapes and frequencies as targets, design variables (including material properties and interface spring stiffnesses) could be refined. This process led to excellent test-analysis correlation in both frequency (within 5% error for relevant modes) and MAC (most modes above 75%). The update also highlighted the importance of including realistic boundary and connection conditions in the FEM, corroborated by experimental observations on the true dynamic response of the stack. The improved FEM, validated against a trustworthy modal reference, forms a solid foundation for structural durability assessment and numerical vibration immunity studies.
- **Fixture Coupling Neutralization:** The experimental results demonstrated clear evidence of fixture coupling, in the form of additional resonances, altered mode shapes, and frequency shifts, especially on the slip table configuration. Various state-of-the-art decoupling techniques (frequency-based, modal-based, and SVD-based) were implemented and evaluated. Their successful application critically depended on the accurate experimental modal model for synthesizing fixed-base characteristics and the selection of the relevant table modes. The SVD-based approach was particularly attractive for its flexibility, though all approaches required careful parameter tuning to avoid over-constraining or losing structural information.
- **Synergies and Research Outlook:** The workflow established in this paper clearly demonstrates that the accuracy of later steps—model updating and fixture decoupling—relies intrinsically on the quality of the experimental modal data. Any uncertainty or error in the modal survey propagates to both FEM correlation and decoupling, and vice versa. Indeed, in the case a fixed-base setup is not available, decoupling is fundamental to identify a modeset to be used for FEM correlation. In turn, a well-updated FEM assists in interpreting residual discrepancies in the test data, separating fixture from structure effects, and refining fixture decoupling procedures. The interplay between accurate experiment, model updating, and decoupling methods is therefore fundamental for robust vibration qualification and design of critical components such as fuel cell stacks for aerospace applications.
- **Recommendations:** Future work should focus on improving the automation and robustness of table mode identification, integrating multi-axial excitation strategies, and extending sensor instrumentation to better capture interface dynamics. Joint consideration of experimental modal analysis, FEM updating, and fixture decoupling in a closed-loop manner can lead to further gains in accuracy and reliability for vibration qualification in demanding engineering scenarios.

Acknowledgments The NEWBORN project is supported by the Clean Aviation Joint Undertaking and its members. Funded by the European Union under Grant Agreement No. 101101967.

Views and opinions expressed are, however, those of the authors only and do not necessarily reflect those of the European Union or Clean Aviation Joint Undertaking. Neither the European Union nor the granting authority can be held responsible for them.

References

1. CORDIS European Commission. “NEWBORN - NExt generation high poWer fuel cells for airBORNe applications”. https://cordis.europa.eu/project/id/101101967/reporting, 2023. Project ID: 101101967.
2. NEWBORN Project Consortium. “NEWBORN Project Official Website”. https://newborn-project.eu/, 2023.
3. PowerCell Group. “PowerCell Sweden AB”. https://powercellgroup.com/.

4. RTCA, Inc. "DO-160G Environmental Conditions and Test Procedures for Airborne Equipment, Section 8 Vibration". Technical report, Federal Aviation Administration, 2010.
5. D. J. Ewins. *Modal Testing: Theory, Practice and Application*. Research Studies Press, Baldock, UK, 2nd edition, 2000.
6. KU Leuven. "The CUBE". https://www.mech.kuleuven.be/en/mod/services-consulting-depreciated/cube.
7. Siemens Digital Industries Software. "Simcenter SCADAS Lab". https://plm.sw.siemens.com/en-US/simcenter/physical-testing/scadas/lab/, 2024.
8. Siemens Digital Industries Software. "Simcenter Testlab". https://plm.sw.siemens.com/en-US/simcenter/physical-testing/testlab/, 2024.
9. Gaëtan Kerschen, Keith Worden, Alexander F. Vakakis, and Jean Claude Golinval. "Past, present and future of nonlinear system identification in structural dynamics". *Mechanical Systems and Signal Processing*, 20(3):505 – 592, 2006.
10. Bart Peeters, Herman Van der Auweraer, Patrick Guillaume, and Jan Leuridan. "The polymax frequency-domain method: A new standard for modal parameter estimation?". *Shock and Vibration*, 11, 2004.
11. Randall J Allemang and David L Brown. "A correlation coefficient for modal vector analysis". *Proceedings of the 1st international modal analysis conference*, 1:110–116, 1982.
12. Herman Van der Auweraer and Dirk Hartmann. "The executable digital twin: merging the digital and the physics worlds". 2023.
13. Giovanni Fasulo, Simone Gallas, Hervé Denayer, Oskar Ekblad, Giancarlo Kosova, and Mattia Barbarino. "A modeling approach for assessing vibration immunity in hydrogen fuel cell stack for aeronautical applications". For submission to *Applied Sciences*, Special Issue: Advances in Aerostructural Analysis, Design, and Optimization., in preparation.
14. "Simcenter Nastran". https://plm.sw.siemens.com/en-US/simcenter/mechanical-simulation/nastran/, 2024.
15. "Simcenter Nastran SOL200 – Structural Optimization". https://plm.sw.siemens.com/en-US/simcenter/mechanical-simulation/nastran/sol200-optimization/, 2024.
16. "Simcenter 3D". https://plm.sw.siemens.com/en-US/simcenter/mechanical-simulation/simcenter-3d/, 2024.
17. Ulrich Füllekrug. "Determination of Effective Masses and Modal Masses from Base- Driven Tests". In *Proceedings of 7th International Congress on Sound and Vibration*, 1996.
18. M. Sinapius. "Identification of Free and Fixed Normal Modes by Base Excitation.". In *Proceedings of 14th International Modal Analysis Conference*, 1996.
19. Carsten Schedlinski and Michael Link. "Identification of Frequency Response Functions and Modal Data from Base Excitation Tests Using Measured Interface Forces". In *Proceedings of the ASME Conference On Noise & Vibration, Boston, Massachusetts*, 1995.
20. Mario Razeto, Jean-Claude Golinval, and Michel Géradin. "Modal Identification and Determination of Effective Mass Using Environmental Vibration Testing on an Electro-dynamic Shaker". In *Proceedings of the 12th International Modal Analysis Conference, Honolulu, Hawaii*, 1994.
21. Thomas G Carne, David R Martinez, and Arlo R Nord. "A comparison of fixed-base and driven-base modal testing of an electronics package". Technical report, Sandia National Labs., Albuquerque, NM (USA), 1989.
22. J.-G. Béliveau, F.R. Vigneron, Y. Soucy, and S. Draisey. "Modal parameter estimation from base excitation". *Journal of Sound and Vibration*, 107(3), 1986.
23. Randy Mayes and Lynn Bridgers. "Extracting Fixed Base Modal Models from Vibration Tests on Flexible Tables". In *Proceedings of the Society for Experimental Mechanics Series*, 2009.
24. Randy Mayes and Mathew Allen. "Converting a Driven Base Vibration Test to a Fixed Base Modal Analysis". In *Proceedings of the 29th International Modal Analysis Conference*, 2011.
25. Benjamin Pacini and R. Mayes. "Computing Effective Mass Using the Modal Craig Bampton Framework". *Experimental Techniques*, 48, 2024.
26. Randy L. Mayes. "Refinements on estimating fixed base modes on a slip table". In *Topics in Modal Analysis I, Volume 5*, pages 359–365, 2012.
27. Peter A. Kerrian. "A Comparison of Different Boundary Condition Correction Methods". In Brandon Dilworth and Michael Mains, editors, *Topics in Modal Analysis & Testing, Volume 8*, 2021.
28. Kevin Napolitano and Nathanael Yoder. "Fixed Base FRF Using Boundary Measurements as References: Analytical Derivation". In *Proceedings of the 30th International Modal Analysis Conference*, 2012.
29. Kevin Napolitano, Nathanael Yoder, and William Fladung. "Extraction of Fixed-Base Modes of a Structure Mounted on a Shake Table". In *Proceedings of the 31st International Modal Analysis Conference*, 2013.
30. Lucas D. Staab, James P. Winkel, Vicente J. Suarez, Trevor M. Jones, and Kevin L. Napolitano. "Fixed Base Modal Testing Using the NASA GRC Mechanical Vibration Facility". In *Proceedings of the 34th International Modal Analysis Conference*, 2016.
31. James Winkel, James Akers, Vicente Suarez, Lucas Staab, and Kevin Napolitano. "Modal Survey of the MPCV Orion European Service Module Structural Test Article Using a Multi-axis Shake Table". In *Proceedings of the 36th International Modal Analysis Conference*, 2017.
32. Kevin L. Napolitano. "Feasibility Study to Extract Artemis-1 Fixed Base Modes While Mounted on a Dynamically Active Mobile Launch Platform". In Chad Walber, Patrick Walter, and Steve Seidlitz, editors, *Sensors and Instrumentation, Aircraft/Aerospace, Energy Harvesting & Dynamic Environments Testing, Volume 7*, 2021.
33. Peter Adam Kerrian and Kevin L. Napolitano. "Pretest Analysis for Modal Survey Tests Using Fixed Base Correction Method". In *Proceedings of the 37th International Modal Analysis Conference*, 2019.
34. Randy L. Mayes, Tyler F. Schoenherr, Jill Blecke, and Daniel P. Rohe. "Efficient Method of Measuring Effective Mass of a System". In *Topics in Experimental Dynamic Substructuring, Volume 2*. Springer New York, 2014.
35. Randy L. Mayes and Matthew S. Allen. "Converting a Driven Base Vibration Test to a Fixed Base Modal Analysis". In Tom Proulx, editor, *Rotating Machinery, Structural Health Monitoring, Shock and Vibration, Volume 5*. Springer New York, 2011.
36. Nathanael Yoder and Kevin Napolitano. "Fixed Base FRF Using Boundary Measurements as References: Experimental Results". In *Proceedings of the 30th International Modal Analysis Conference*, 2012.
37. Natalie Spivey, Rachel Saltzman, Carol Wieseman, Kevin Napolitano, and Benjamin Smith. *Passive Aeroelastic Tailored Wing Modal Test Using the Fixed Base Correction Method*, pages 61–83. Springer International Publishing, 2021.